



This discussion paper is/has been under review for the journal Geoscientific Model Development (GMD). Please refer to the corresponding final paper in GMD if available.

# A strategy for GIS-based 3-D slope stability modelling over large areas

M. Mergili<sup>1</sup>, I. Marchesini<sup>2</sup>, M. Alvioli<sup>2</sup>, M. Metz<sup>3</sup>, B. Schneider-Muntau<sup>4</sup>,  
M. Rossi<sup>2,5</sup>, and F. Guzzetti<sup>2</sup>

<sup>1</sup>Institute of Applied Geology, BOKU University, Vienna, Austria

<sup>2</sup>CNR-IRPI, Perugia, Italy

<sup>3</sup>Fondazione Edmund Mach, San Michele all'Adige, Italy

<sup>4</sup>Division of Geotechnical and Tunnel Engineering, University of Innsbruck, Austria

<sup>5</sup>Department of Geosciences, University of Perugia, Italy

Received: 20 June 2014 – Accepted: 28 July 2014 – Published: 11 August 2014

Correspondence to: M. Mergili (martin.mergili@boku.ac.at)

Published by Copernicus Publications on behalf of the European Geosciences Union.

GMDD

7, 5407–5445, 2014

A strategy for  
GIS-based 3-D slope  
stability modelling

M. Mergili et al.

Title Page

Abstract

Introduction

Conclusions

References

Tables

Figures



Back

Close

Full Screen / Esc

Printer-friendly Version

Interactive Discussion



## Abstract

GIS-based deterministic models may be used for landslide susceptibility mapping over large areas. However, such efforts require specific strategies to (i) keep computing time at an acceptable level, and (ii) parameterize the geotechnical data. We test and optimize the performance of the GIS-based, 3-D slope stability model `r.slope.stability` in terms of computing time and model results. The model was developed as a C- and Python-based raster module of the open source software GRASS GIS and considers the 3-D geometry of the sliding surface. It calculates the factor of safety (FoS) and the probability of slope failure ( $P_f$ ) for a number of randomly selected potential slip surfaces, ellipsoidal or truncated in shape. Model input consists of a DEM, ranges of geotechnical parameter values derived from laboratory tests, and a range of possible soil depths estimated in the field. Probability density functions are exploited to assign  $P_f$  to each ellipsoid. The model calculates for each pixel multiple values of FoS and  $P_f$  corresponding to different sliding surfaces. The minimum value of FoS and the maximum value of  $P_f$  for each pixel give an estimate of the landslide susceptibility in the study area. Optionally, `r.slope.stability` is able to split the study area into a defined number of tiles, allowing parallel processing of the model on the given area. Focusing on shallow landslides, we show how multi-core processing allows to reduce computing times by a factor larger than 20 in the study area. We further demonstrate how the number of random slip surfaces and the sampling of parameters influence the average value of  $P_f$  and the capacity of `r.slope.stability` to predict the observed patterns of shallow landslides in the 89.5 km<sup>2</sup> Collazzone area in Umbria, central Italy.

## 1 Introduction

Landslide susceptibility is the spatial probability of landslide occurrence, based on local terrain conditions (Brabb, 1984; Guzzetti et al., 1999). The susceptibility to landslides can be determined using statistical and physically-based models (Guzzetti et al., 1999;

## A strategy for GIS-based 3-D slope stability modelling

M. Mergili et al.

[Title Page](#)

[Abstract](#)

[Introduction](#)

[Conclusions](#)

[References](#)

[Tables](#)

[Figures](#)

◀

▶

◀

▶

[Back](#)

[Close](#)

[Full Screen / Esc](#)

[Printer-friendly Version](#)

[Interactive Discussion](#)



Van Westen, 2000; Guzzetti, 2006; Van Westen et al., 2006). Most commonly, modelling of the spatial probability of shallow landslides for small catchments relies upon the use of physically-based (“deterministic”) models (Van Westen et al., 2006). These models build on the limit equilibrium concept, and assume (i) slopes consisting of rigid materials, (ii) a Coulomb (1776) mechanical model for the slope materials applies, and (iii) the possible rupture occurrence along single failure planes i.e., the slip surface. The factor of safety (Carson and Kirkby, 1972; Crozier, 1986; Duncan and Wright, 2005) of the failure plane measures the stability/instability conditions of the slope. It is given by the dimensionless ratio between the resisting (stabilizing) forces  $R$ , and the driving (destabilizing) forces  $T$ , or

$$\text{FoS} = \frac{R}{T}. \quad (1)$$

Where  $\text{FoS} > 1$ , the slope is considered stable.  $\text{FoS} = 1$  represents meta-stable conditions, and  $\text{FoS} < 1$  corresponds to unrealistic physical conditions where the driving forces exceed the resisting forces, and is taken to indicate an unstable slope (Raia et al., 2014).

The infinite slope stability model is commonly used when applying the limit equilibrium concept in a raster Geographical Information system (GIS). This simple approach is often coupled with more or less complex hydraulic and infiltration models. The latter are used to predict the location and timing of failures in an area in response to precipitation (Montgomery and Dietrich, 1994; Pack et al., 1998; Wilkinson et al., 2002; Xie et al., 2004a; Godt et al., 2008; Muntohar and Liao, 2010; Raia et al., 2014). Raia et al. (2014) have proposed a probabilistic modification of TRIGRS (Baum et al., 2002, 2008, 2010), where probability distributions for the required geotechnical and hydraulic parameters are used as the input variables, and a probabilistic interpretation of the results of the calculations of the spatially-distributed values of FoS is suggested.

The infinite slope stability model assumes a planar slope of infinite length, with the potential failure plane parallel to the topographic surface. In a raster GIS, calculation of FoS for each individual pixel is straightforward. The forces acting between the pixels

## A strategy for GIS-based 3-D slope stability modelling

M. Mergili et al.

[Title Page](#)

[Abstract](#)

[Introduction](#)

[Conclusions](#)

[References](#)

[Tables](#)

[Figures](#)



[Back](#)

[Close](#)

[Full Screen / Esc](#)

[Printer-friendly Version](#)

[Interactive Discussion](#)



<a href="#">Title Page</a>	
<a href="#">Abstract</a>	<a href="#">Introduction</a>
<a href="#">Conclusions</a>	<a href="#">References</a>
<a href="#">Tables</a>	<a href="#">Figures</a>
<a href="#">Full Screen / Esc</a>	
<a href="#">Printer-friendly Version</a>	
<a href="#">Interactive Discussion</a>	

are ignored since the failure is assumed to be infinitely wide and long. This has facilitated the widespread application of this type of model (Van Westen and Terlien, 1996; Burton and Bathurst, 1998; Xie et al., 2004a; Baum et al., 2008; Godt et al., 2008; Raia et al., 2014). However, the infinite slope stability model is well suited only for shallow slope stability in frictional materials, and is less appropriate for cohesive materials (Mergili et al., 2014). Further, the infinite slope stability model fails to capture the complexity of deep-seated and complex landslides. Milledge et al. (2012) determined that the infinite length assumption is always reasonable for landslides with a length-to-depth ratio  $L/D > 25$ , whereas Griffiths et al. (2011) give a threshold  $L/D = 16$ .

Shallow slope failures coexist locally with deep-seated mass movements (Guzzetti et al., 2004, 2006a; Zézere et al., 2005). To evaluate the stability/instability conditions of slopes susceptible to deep-seated landslides, more complex limit equilibrium models should be used. Such models were developed and are applied commonly to two-dimensional cross sections drawn along the steepest terrain gradient (Duncan and Wright, 2005). The zone above a known, inferred, or hypothetical failure plane is divided into vertical slices of equal or different sizes.  $R$  and  $T$  are computed for each slice, and summed up linearly to obtain a single value of FoS for the entire slope. Most commonly, the forces acting between the slices are neglected (Fellenius, 1927). In many cases, this simplification leads to a lower value of FoS (Kolymbas, 2007). Fellenius (1927), Bishop (1954), Janbu et al. (1956), and Morgenstern and Price (1967) have proposed different schemes to calculate the FoS along pre-defined slope profiles and associated failure planes. Later, this type of model was extended to 3-D topographies and failure planes (e.g., Hovland, 1977; Hungr, 1987; Hungr et al., 1989).

Specific software packages were designed to test multiple 3-D failure planes, searching for the lowest FoS value e.g., CLARA (Hungr, 1988), TSLOPE3 (Pyke, 1991), or 3D-SLOPE (Lam and Fredlund, 1993). The different software were designed to model individual slopes, or portions of a slope, and cannot be used effectively for a broad-scale (regional) analysis of the slope stability conditions. Commonly, one refers to large areas when hundreds of millions of pixels have to be processed. With regard

<a href="#">Title Page</a>	
<a href="#">Abstract</a>	<a href="#">Introduction</a>
<a href="#">Conclusions</a>	<a href="#">References</a>
<a href="#">Tables</a>	<a href="#">Figures</a>
<a href="#">◀</a>	<a href="#">▶</a>
<a href="#">◀</a>	<a href="#">▶</a>
<a href="#">Back</a>	<a href="#">Close</a>
<a href="#">Full Screen / Esc</a>	
<a href="#">Printer-friendly Version</a>	
<a href="#">Interactive Discussion</a>	



to 3-D slope stability modelling, we consider any area larger than a single slope as a large area. Few attempts were made to develop sliding surface models applicable at the regional scale, coupled to GIS (Reid et al., 2000; Xie et al., 2003, 2004b, 2004c, 2006; Marchesini et al., 2009; Jia et al., 2012). A recent study of Mergili et al. (2014) indicates that, also for shallow landslides, more complex slip surface models might perform slightly better in reproducing the observed landslide areas than the infinite slope stability model.

The GIS implementation of limit equilibrium models more complex than the simple infinite slope stability model remains challenging. At the regional scale, a very large number of possible slip surfaces has to be tested, using a reasonably fine pixel spacing. For the purpose, efficient computing strategies are needed to avoid unacceptably long computing times. In this work, we propose an implementation of a 3-D sliding surface model where the study area is partitioned into overlapping tiles, processed in parallel on a multi-core computer. For our experiment, we use the model r.slope.stability, a further development of r.rotstab (Mergili et al., 2014), to demonstrate strategies to optimize model performance in terms of computing time and of the quality of the model results. r.slope.stability was implemented as a raster module of the open source software package GRASS GIS (Neteler and Mitasova, 2007; GRASS Development Team, 2014). GRASS GIS is well suitable for the task due to its open structure, modular design, and the compatibility with various programming languages. Further, GRASS GIS is frequently used as the basis for GIS-based models related to mass movements (Mergili et al., 2012a, b, 2014; Gruber and Mergili, 2013). Our parallel implementation is performed at the Python level, whereas the core of the model is written in C. The model code and a user manual can be obtained from the model's web site <http://www.slopeability.org>.

In the following sections, we first introduce the 3-D (strictly speaking, 2.5-D, as the vertical dimension is represented by attributes, not by coordinates) slope stability model r.slope.stability (Sect. 2). We then present the study area and the data used in the experiment (Sect. 3), and we define the framework for testing the performance of the

software in terms of quality of the model results and computing time (Sect. 4). Next, we present (Sect. 5) and discuss (Sect. 6) the results before concluding with the key messages of the work (Sect. 7).

## 2 The r.slope.stability model

### 5 2.1 Modelling approach

Given a digital elevation model (DEM) and a set of geotechnical and geometric parameters, the r.slope.stability model evaluates the slope stability conditions for a large number of randomly selected ellipsoidal or truncated slip surfaces (Fig. 1). The ellipsoidal slip surfaces are defined by the geographical coordinates of the centre, the length of the three half axes  $a_e$ ,  $b_e$  and  $c_e$ , the aspect  $\alpha$ , the inclination  $\beta$ , and the offset of the ellipsoid centre above the terrain. The  $a_e$  half axis follows the steepest slope, and  $c_e$  is aligned perpendicular to the terrain surface. The slope stability calculation is executed using user-defined parameters of landslide length  $L$ , landslide width  $W$ , maximum depth of the bottom of the ellipsoid  $D$ , and offset of the ellipsoid centre above the terrain  $z_b$  (relative to  $c_e$ ). Alternatively, the calculation may be performed using randomized ellipsoid parameters, constrained by user-defined minimum and maximum values of the parameters. The second option is particularly suitable for testing a large number of slip surfaces. The tested slip surfaces correspond well to ideal ellipsoids only for reasonably small pixels in relation to the ellipsoid size. When using larger pixels, the shapes of the tested slip surfaces represent systems of discrete plane surfaces strongly depending on the discretization of the pixels. For the modelling of more realistic shallow failure planes, r.slope.stabiliy can use truncated ellipsoids to consider the bottom of soil, shallow weak layers, or shallow discontinuities bounded by hard bedrock as possible failure planes. As a consequence, more than one slip surface may be associated to each ellipsoid (Mergili et al., 2014).

A strategy for  
GIS-based 3-D slope  
stability modelling

M. Mergili et al.

[Title Page](#)

[Abstract](#)

[Introduction](#)

[Conclusions](#)

[References](#)

[Tables](#)

[Figures](#)

◀

▶

◀

▶

[Back](#)

[Close](#)

[Full Screen / Esc](#)

[Printer-friendly Version](#)

[Interactive Discussion](#)



To compute FoS, r.slope.stability adopts a modified version of the 3-D sliding surface model of Hovland (1977), revised and extended by Xie et al. (2003, 2004b, c, 2006):

$$\text{FoS} = \frac{\sum_C (c' \cdot A + (G' \cos \beta_c + N_s) \tan \varphi') \cos \beta_m}{\sum_C (G' \sin \beta_m + T_s) \cos \beta_m}. \quad (2)$$

In Eq. (2), the upper term corresponds to the resisting forces  $R$ , and the lower term corresponds to the driving forces  $T$  (see Eq. 1).  $R$  and  $T$  are summed over all columns  $C$  of the slip surface.  $c'$  ( $\text{N m}^{-2}$ ) is the effective cohesion,  $A$  ( $\text{m}^2$ ) is the 3-D area of the slip surface of the considered pixel,  $G'$  ( $\text{N}$ ) is the weight of the moist soil,  $\beta_c$  is the inclination of the slip surface at the considered column,  $\varphi'$  is the effective internal friction angle, and  $\beta_m$  is the apparent dip of the slip surface at the considered column in the direction of  $\alpha$ .  $N_s$  and  $T_s$  ( $\text{N}$ ) are the contributions of the seepage force to the normal force and the shear force. Additional external forces, such as seismic loading, are not considered by the model. The geotechnical, hydraulic, and geometric principles of the FoS calculation are discussed in detail by Mergili et al. (2014).

Upon completion of the slope stability calculation for all the slip surfaces, each pixel in the modelling domain is intersected by various slip surfaces, and each slip surface is associated with a value of FoS. For each pixel, the lowest value of FoS of all the intersecting slip surfaces is taken as the representative FoS.

Compared to the r.rotstab model (Mergili et al., 2014), r.slope.stability introduces the following innovations:

- 20 1. An improved data management strategy to meet the standards of GRASS GIS, including built-in functions for model validation and graphic presentation.
2. The ability to fully exploit multi-core computers.
3. The ability to consider complex systems of geological layers, relevant for the modelling of deep-seated landslides.

<a href="#">Title Page</a>	
<a href="#">Abstract</a>	<a href="#">Introduction</a>
<a href="#">Conclusions</a>	<a href="#">References</a>
<a href="#">Tables</a>	<a href="#">Figures</a>
<a href="#">◀</a>	<a href="#">▶</a>
<a href="#">◀</a>	<a href="#">▶</a>
<a href="#">Back</a>	<a href="#">Close</a>
<a href="#">Full Screen / Esc</a>	
<a href="#">Printer-friendly Version</a>	
<a href="#">Interactive Discussion</a>	



4. The ability to compute the slope failure probability  $P_f$  in addition to FoS, based on the statistical distribution of  $c'$ ,  $\varphi'$  and, for truncated ellipsoids, the truncated depth  $d$ .

Points (1) and (2) are explained in Sect. 2.2, and point (3) is not exploited in this work.

5. The rationale of point (4) relies on the high natural variability of the geotechnical parameters, resulting in an uncertain definition of the horizontal and vertical distributions of  $c'$  and  $\varphi'$  (see Sect. 3). A map of FoS building on data from a single site, or a limited number of sites, may fail to account for the details of the landscape. To overcome this limitation, we adopt an approach to compute the slope failure probability  $P_f$ . This 10 approach allows considering the full range of measured values of  $c'$  and  $\varphi'$ . The statistical properties of the parameters are assumed constant in space (see Sect. 6). A range of values of the truncated depth  $d$  can be considered, which is particularly useful for modelling shallow landslides in soils of uncertain depth. This approach is implemented in the following three steps:
- 15 1. Computing the arithmetic mean  $\mu$ , standard deviation  $\sigma$ , minima and maxima of  $c'$ ,  $\varphi'$  and  $d$ . The number of samples  $n$  of parameter combinations to be collected is defined by the user.
- 20 2.  $c'$ ,  $\varphi'$  and  $d$  are varied as a function of the defined minima, maxima and intervals in order to exploit the full range of possible parameter values. The variation of  $d$  builds on truncating the ellipsoid at various depths. FoS is computed for each combination using Eq. (2), building the ratio of the sums of the shear resistances and the shear forces over all columns of the ellipsoid (see Fig. 1).
- 25 3. The slope failure probability  $P_f$  for the ellipsoid is computed as a function of the fraction of parameter combinations where  $\text{FoS} < 1$ , related to all the tested parameter combinations:

$$P_f = \sum_{i=1}^n f_i \cdot w_i, \quad (3)$$

## A strategy for GIS-based 3-D slope stability modelling

M. Mergili et al.

[Title Page](#)

[Abstract](#)

[Introduction](#)

[Conclusions](#)

[References](#)

[Tables](#)

[Figures](#)



[Back](#)

[Close](#)

[Full Screen / Esc](#)

[Printer-friendly Version](#)

[Interactive Discussion](#)



where  $f_i = 1$  for  $\text{FoS}_i < 1$ ,  $f_i = 0$  for  $\text{FoS}_i \geq 1$ , and  $w_i$  is the weight assigned to the parameter combination  $i$  (see below). The sum of  $w_i$  over all parameter combinations  $n$  is 1.

At the end, the largest value of  $P_f$  out of all intersecting slip surfaces is taken as the value representative for each pixel.  
5

The sample of parameters to be tested has to represent the probability of occurrence of the parameter combination. Figure 2 illustrates three possible strategies, using a sample size of  $n = 100$  for two normally distributed, arbitrary parameters. (a) Random sampling of parameter combinations: 100 parameter combinations are randomly sampled, where the probability of a parameter combination to be sampled directly relates to the product of the probability densities of the parameter values. (b) Random sampling of parameters. Here, 10 values of each parameter are randomly sampled, where the probability of a parameter value to be sampled directly relates to its probability density. All possible pairs of sampled parameter values are then considered, resulting in 100 tests. (c) Equal density sampling. Ten values of each parameter are sampled, equally distributed along the cumulative density function associated to each parameter (see Fig. 2d). This ensures that the distribution of samples reflects the PDF. All possible pairs of sampled parameter values are then considered, resulting in a total number of 100 tests.  
10  
15

With (a) or (b),  $w_i = 1/n$  (see Eq. 3) and the samples are determined separately for each ellipsoid. With (c), one sample is used for all ellipsoids.  $w_i$  represents the product of the cumulative density intervals associated to the values of the combined parameters (see Fig. 2d). This means that the edge samples are down-weighted as they only represent half of the area under the PDF, compared to the other samples.  
20

This approach can equally be applied to three ( $c'$ ,  $\varphi'$ ,  $d$ ) instead of two ( $c'$ ,  $\varphi'$ ) parameters. Four types of PDFs can be used: rectangular, normal, log-normal or exponential (see Sect. 4).  
25

---

## A strategy for GIS-based 3-D slope stability modelling

---

M. Mergili et al.

[Title Page](#)

[Abstract](#)

[Introduction](#)

[Conclusions](#)

[References](#)

[Tables](#)

[Figures](#)

[◀](#)

[▶](#)

[◀](#)

[▶](#)

[Back](#)

[Close](#)

[Full Screen / Esc](#)

[Printer-friendly Version](#)

[Interactive Discussion](#)



## 2.2 Computational implementation

r.slope.stability is a raster module of the open source software package GRASS GIS 6.4 (Neteler and Mitasova, 2007; GRASS Development Team, 2014). The software exploits the Python programming language for data management, pre-processing and post-processing tasks. The slope stability model itself (see Sect. 2.1) is implemented as a C code (sub-module r.slope.stability.main). r.slope.stability also includes a built-in validation and presentation module. Output maps and plots are produced using R, a free software environment for statistical computing and graphics (R Core Team, 2014). The logical framework of r.slope.stability is illustrated in Fig. 3.

The numerical implementation presented in this work extends the applicability of the slope stability model to large study areas. This requires a very large number of ellipsoids to be tested. Assuming a test site with an area of  $100 \text{ km}^2$ , average ellipsoids of length  $L_{\text{avg}} = 100 \text{ m}$  and width  $W_{\text{avg}} = 80 \text{ m}$ , and an average number of ellipsoids per pixel (the “density” of ellipsoids)  $d_e = 1000$ , the total number of ellipsoids  $n_e$  to be tested sums up to roughly 16 million,

$$n_e \approx d_e \frac{A}{(\pi/4) \cdot L_{\text{avg}} \cdot W_{\text{avg}}} \quad (4)$$

The pixel spacing used for the slope stability model has to be small enough to capture the geometry of the assumed slope failure, which may fall into a very broad range of sizes (see e.g., Alvioli et al., 2014, and references therein). Given a study area of  $100 \text{ km}^2$  and a pixel size of 5 m, four million pixels need to be processed. The potentially large number of pixels in combination with the large number of ellipsoids, and the complex processing of each ellipsoid, pose challenges in terms of (i) computer memory and (ii) computing time. We combine two strategies to overcome these computational challenges:

- 25 1. In the C programming environment, raster datasets are commonly held in memory as arrays. This allows a fast and efficient access to each pixel. If the datasets

[Title Page](#)[Abstract](#)[Introduction](#)[Conclusions](#)[References](#)[Tables](#)[Figures](#)[◀](#)[▶](#)[◀](#)[▶](#)[Back](#)[Close](#)[Full Screen / Esc](#)[Printer-friendly Version](#)[Interactive Discussion](#)

5 become too large, or if too many large arrays are held in memory at the same time, the available memory may be exceeded, causing the model execution to fail. We use the GRASS GIS Segment Library (GRASS Development Team, 2014) to avoid this problem. The library enables storage and use of very large raster datasets independently from the available computer memory, however at the expense of computing time. `r.slope.stability.main` uses the GRASS Segment Library for data input, preparation, and output. For ellipsoid-specific computations, where a lot of data covering a smaller number of pixels has to be accessed frequently, it uses arrays by default. In this study, we apply a segment size of  $16 \times 16$  pixels to all computations, maintaining 16 segments in memory. As the most time-consuming operations of `r.slope.stability` make only limited use of the GRASS Segment Library, preliminary studies have shown that, within a certain range, the computing time displays a weak dependence on changes in those settings.

- 10
- 15
- 20
- 25
2. To reduce the computing time when modelling the slope stability of large areas, `r.slope.stability` provides the option to divide the study area into a user-defined number of tiles processed in parallel, if the code is run on an ordinary multi-processor or multi-core machine (see Fig. 3). In this case, `r.slope.stability.main` is run separately for each tile. The final result is obtained by collecting and combining the results for the single tiles. To ensure a full coverage of the study area, an overlap between the tiles of at least the maximum ellipsoid dimension is required. Each tile is sent to a free computing core as soon as one is available, and until all the tiles are processed. This procedure is implemented in the way that the `r.slope.stability.py` module produces a batch file for each tile. The batch file calls the sub-module `r.slope.stability.multicore`, which is then used to launch `r.slope.stability.main` with the tile-specific parameters (see Fig. 3); the actual parallel processing is performed in the Python part of the module, exploiting the “Threading” Python library (a higher-level threading interface) and the “Queue” Python module (a class for managing the “producer-consumer” problem able to block execution until all the items in the queue have been processed).

---

## A strategy for GIS-based 3-D slope stability modelling

M. Mergili et al.

---

[Title Page](#)

[Abstract](#)

[Introduction](#)

[Conclusions](#)

[References](#)

[Tables](#)

[Figures](#)



[Back](#)

[Close](#)

[Full Screen / Esc](#)

[Printer-friendly Version](#)

[Interactive Discussion](#)



We note that neither the use of the GRASS Segment Library nor multi-core processing affect the model results in terms of Fos or  $P_f$ .

### 3 Study area and data

We test the r.slope.stability code in the Collazzone area, Umbria, central Italy (Fig. 4).

- Covering an area of  $89.5 \text{ km}^2$ , this hilly area ranges from 145 m a.s.l. along the Tiber River flood plain, to 634 m a.s.l. at Monte di Grutti. Various types of continental sediments, Pliocene to Pleistocene in age, cover the area. Landslides are frequent and abundant in the Collazzone area, and a detailed landslide inventory (Fig. 4) is available along with geologic and morphologic information and maps (Guzzetti et al., 2006a, b, 2009; Ardizzone et al., 2007; Galli et al., 2008; Rossi et al., 2010; Fiorucci et al., 2011). Intense or prolonged rainfall periods are the primary natural triggers of landslides in the area (Ardizzone et al., 2013), followed by rapid snow melt (Cardinali et al., 2000). Recent landslides are most frequent in cultivated areas, indicating a relationship with agricultural practices.

In the present work we focus on shallow landslides, considering an inventory of 2381 landslides (Fig. 4) for model evaluation (see Sect. 5). The 5th and 95th percentiles of landslide length  $L$ , width  $W$ , and of the  $L/W$  ratio for selected shallow landslides are used for constraining the randomization of possible slip ellipsoids (Table 1; see Sect. 4).

Most commonly, the sliding surface of shallow landslides coincides with the lower boundary of the soil which, in cultivated areas, we define as the layer disturbed by agricultural practices. Statistics of soil depth  $d_s$  in the continental sediments of the Collazzone area were obtained from a set of 90 measurements, considering the lower boundary of the  $C_v$  horizon, where present. Analysis of the measurements resulted in an arithmetic mean of the soil depth  $\mu = 0.60 \text{ m}$ , with a standard deviation  $\sigma = 0.27 \text{ m}$ . The minimum soil depth measured in the area was zero, and the maximum soil depth was 1.22 m.

<a href="#">Title Page</a>	
<a href="#">Abstract</a>	<a href="#">Introduction</a>
<a href="#">Conclusions</a>	<a href="#">References</a>
<a href="#">Tables</a>	<a href="#">Figures</a>
<a href="#">◀</a>	<a href="#">▶</a>
<a href="#">◀</a>	<a href="#">▶</a>
<a href="#">Back</a>	<a href="#">Close</a>
<a href="#">Full Screen / Esc</a>	
<a href="#">Printer-friendly Version</a>	
<a href="#">Interactive Discussion</a>	



Figure 4 illustrates that landslides are rare where hard bedrock crops out (hatched areas), and abundant in the continental sediments (all other areas). In the present work, we consider all areas with hard bedrock outcrops as unconditionally stable, and concentrate to the areas where continental sediments crop out. The geotechnical characteristics of the continental sediments in the study area were estimated using direct shear tests on 13 samples taken from a variety of lithological conditions (Table 2, see Fig. 4). The variation of geotechnical parameters within each class is considerable, partly exceeding the variation between the classes. For this reason, we decide not to consider separate sets of geotechnical parameters for the different lithological classes present in the study area. Instead, we explore the statistics of the parameters for the entire area with continental sediments. The same approach is used for the parameterization of the soil depth.

In addition to the landslide inventory, soil depths, and the geotechnical data, we use a  $5\text{ m} \times 5\text{ m}$  digital elevation model (DEM) derived by the automatic interpolation of 10 m and 5 m contour lines, obtained from 1 : 10 000 scale topographic base maps.

## 4 Model parameterization

In this work, we consider only shallow slope stability, truncating the ellipsoids at the depth of the soil. We set the dry specific weight of the soil  $\gamma_d = 15.8\text{ kN m}^{-3}$  (see Table 2), and the saturated water content  $\Theta_s = 40\text{ vol.-\%}$ . Within a reasonable range of values, both parameters are not decisive for the outcome of the slope stability computation. Instead, FoS and  $P_f$  are most sensitive to the effective cohesion  $c'$ , the effective angle of internal friction  $\varphi'$ , the depth of the potential failure plane  $d$  and the water status of the soil. We use the following parameterization for computing  $P_f$  (see Eq. 3):

1. We calculate the arithmetic mean of  $c'$  from field data reported in Table 2. Then, we assume an exponential PDF to model the variability of  $c'$  (El-Ramly et al., 2005; Petrovic, 2008).

<a href="#">Title Page</a>	
<a href="#">Abstract</a>	<a href="#">Introduction</a>
<a href="#">Conclusions</a>	<a href="#">References</a>
<a href="#">Tables</a>	<a href="#">Figures</a>
<a href="#">◀</a>	<a href="#">▶</a>
<a href="#">◀</a>	<a href="#">▶</a>
<a href="#">Back</a>	<a href="#">Close</a>
<a href="#">Full Screen / Esc</a>	
<a href="#">Printer-friendly Version</a>	
<a href="#">Interactive Discussion</a>	



2. For  $\varphi'$ , we assume a log-normal PDF (El-Ramly et al., 2005) which parameters (mean and standard deviation) are derived from field data (see Table 2).
- 5 3. As commonly observed for shallow landslides in the Collazzone area, the maximum slip surface depth – at which all ellipsoids are truncated – is set to the soil depth. A log-normal PDF is used to model the variability of truncated depth.
- 10 4. We further assume the hydraulically most unfavourable case of fully saturated soil with slope-parallel seepage.

A separate map of FoS is computed, considering the most probable values (modes) of  $c'$ ,  $\varphi'$  and truncated depth  $d$ , deriving those from their respective PDF:  $c' = 0 \text{ kN m}^{-2}$ ;  $10 \varphi' = 27.3^\circ$ ;  $d = 0.46 \text{ m}$ .

Table 2 lists a range of  $c' = 0\text{--}24.5 \text{ kN m}^{-2}$  and  $\varphi' = 18.1\text{--}42.4^\circ$ . These values are used to constrain the variation of the parameters during r.slope.stability runs. For  $c'$  and  $\varphi'$ , this range is justified by the rule-of-thumb values given by Prinz and Strauss (2011) for the possible range of geotechnical parameters for various soil types: for the 15 continental sediments in the Collazzone area the relevant ranges would be  $c' = 0\text{--}25 \text{ kN m}^{-2}$  and  $\varphi' = 15\text{--}45^\circ$ . For the soil depth  $d$ , the maximum of 1.22 m corresponds reasonably well to the approximately 1.3 m maximum depth of disturbance by agricultural practices observed in the Collazzone area (Mergili et al., 2014). Table 3 summarizes the parameters' minima, maxima, and assumed statistical distributions used for the computation of  $P_f$ . The geotechnical parameterization is kept constant for all the 20 tests.

Table 4 lists the parameters tested, and the settings applied in our numerical experiments. The ellipsoid size is constrained according to Table 1. The maximum depth of the bottom of the ellipsoid is constrained with  $D = 2.5\text{--}10 \text{ m}$ . Considering all the combinations of the parameter values listed in Table 4 would result in a very large number 25 of model runs, with excessive computing times. We therefore divide the task into two parts:

7, 5407–5445, 2014

**A strategy for  
GIS-based 3-D slope  
stability modelling**

M. Mergili et al.

[Title Page](#)

[Abstract](#)

[Introduction](#)

[Conclusions](#)

[References](#)

[Tables](#)

[Figures](#)



[Back](#)

[Close](#)

[Full Screen / Esc](#)

[Printer-friendly Version](#)

[Interactive Discussion](#)



1. Multi-core processing: influence of multi-core processing on the computing time  
of  $r.\text{slope}.\text{stability}$  for the entire Collazzone area (Fig. 4). A few combinations of  
the number of tiles  $t$ , and the number of processors  $p$  given in Table 4 are tested  
for  $d_e = 100$  and  $2500$ , and  $d_x = d_y = 5$  m.

5      2. Factor of safety and slope failure probability: influence of  $d_e$  and – in the case of  $P_f$   
– sample size  $n$  (number of tested values of  $c'$ ,  $\varphi'$  and  $d$ ) and sampling strategy  
(see Fig. 2) – on the model results (average value of  $P_f$  and correspondence with  
observed shallow landslides). Part of this test is performed for a subset of the  
Collazzone area (see Fig. 4). All possible values of  $d_e$  and  $n$  given in Table 4 are  
considered.

10

## 5 Results

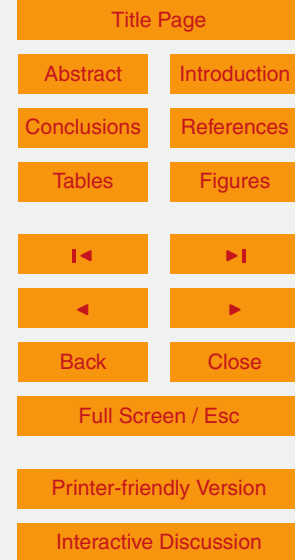
### 5.1 Test 1: multi-core processing

The gain in computing time due to parallel processing is most easily summarized by  
the speedup  $S_p$ :

$$15 \quad S_p = \frac{T_0}{T_p} = \frac{1}{f_s + f_p/p}, \quad (5)$$

where  $p$  is the number of processes,  $T_0$  is the execution time of the sequential algorithm,  
 $T_p$  is the execution time of the parallel algorithm with  $p$  processes,  $f_s$  is the  
sequential fraction, summarizing the overhead, or irreducible serial part, of the code,  
and  $f_p$  is the parallel fraction ( $f_s + f_p = 1$ ).  $S_p = p$  or  $f_s = 1 - f_p = 0$  would indicate a linear  
or ideal speedup. In such a case, the efficiency  $E_p$

$$20 \quad E_p = \frac{T_0}{p \cdot T_p} \quad (6)$$



## A strategy for GIS-based 3-D slope stability modelling

M. Mergili et al.

<a href="#">Title Page</a>	
<a href="#">Abstract</a>	<a href="#">Introduction</a>
<a href="#">Conclusions</a>	<a href="#">References</a>
<a href="#">Tables</a>	<a href="#">Figures</a>
<a href="#">◀</a>	<a href="#">▶</a>
<a href="#">◀</a>	<a href="#">▶</a>
<a href="#">Back</a>	<a href="#">Close</a>
<a href="#">Full Screen / Esc</a>	
<a href="#">Printer-friendly Version</a>	
<a href="#">Interactive Discussion</a>	

would be 1.  $f_s > 0$  and  $E_p < 1$  in the case of r.slope.stability due to (i) shared use of the RAM by multiple cores, (ii) non-optimized sequential use of cores, (iii) operations such as creating tiles and combining the results from each single tile. Further, the total area to be processed increases with  $t$  due to the overlap between the tiles.

We now show the patterns of  $f_s$ ,  $S_p$  and  $E_p$  when using r.slope.stability to compute FoS for the entire Collazzone area at a pixel size of  $5\text{ m} \times 5\text{ m}$ , constraining the ellipsoid size according to Table 1. Figure 5 clearly illustrates that the values of  $f_s$ ,  $S_p$  and  $E_p$  depend on  $t$ ,  $p$  and  $d_e$ . Figure 5a–c illustrate  $f_s$ ,  $S_p$  and  $E_p$  for  $d_e = 100$ . The graphs clearly reflect high values of  $f_s$  for high values of  $t$ . Consequently, speedup and efficiency are highest with relatively low values of  $t$  (42).  $f_s$  is much lower with  $d_e = 2500$ , resulting in optimum values of  $S_p$  and  $E_p$  using a large number of tiles (see Fig. 5d–f). These observations are easily explained by the fact that speedup and efficiency are turned down with large values of  $t$  by the high cost of combining the results from the different tiles into one set of raster maps for the entire study area. The relative impact of this effect – and therefore also  $f_s$  – decreases with increasing values of  $d_e$ . With  $d_e = 2500$ , the optimum speedup and efficiency are observed with 182 tiles.  $S_p$  does not follow a linear increase with  $p$ , reflected in decreasing values of  $E_p$  with  $p$  (see Fig. 5c and f). This phenomenon is most likely explained by the shared use of the RAM by multiple cores.

Further, we note that there is no gain in terms of speedup at  $p > t$  (not shown in Fig. 5). However, for the lower values of  $t$ , speedup becomes constant with increasing  $p$  already at  $p < t$ . This observation reflects a non-optimized sequential use of cores. Particularly with low values of  $p$  or  $t$ , and varying numbers of null cells among the tiles, it likely happens that one core is assigned much more work load than another. This type of effects, illustrated by the irregular patterns of  $E_p$  at lower values of  $t$ , is smoothed out at high values of  $t$ , where load balance is roughly done automatically. This phenomenon also results in increasing values of  $S_p$  for  $t > p$ .

The effects of considering other study areas, different pixel sizes or different ellipsoid dimensions on  $T_p$  have to be noted. In principle, we expect a near-linear dependency of

[Title Page](#)[Abstract](#)[Introduction](#)[Conclusions](#)[References](#)[Tables](#)[Figures](#)[◀](#)[▶](#)[◀](#)[▶](#)[Back](#)[Close](#)[Full Screen / Esc](#)[Printer-friendly Version](#)[Interactive Discussion](#)

$T_p$  on the number of pixels to be processed. However, increasing the pixel size results in an under-proportional gain of  $T_p$ . Areas of null cells due to the irregular shape of the study area cause computations on ellipsoids or entire tiles to break in an early stage of processing. This leads to a relative increase of operations not depending on the 5 number of pixels.

We further expect that the computing time does not depend on the dimensions of the ellipsoids: a given value of  $d_e$  means that all pixels of the study area have to be considered for approx.  $d_e$  times (see Eq. 4). If larger ellipsoid dimensions are chosen, fewer ellipsoids need to be processed. However, larger ellipsoids have a higher chance 10 to be cancelled as they touch areas with null cells rather than smaller ellipsoids. As a consequence,  $T_p$  decreases with larger ellipsoids. In the specific setting considered here, doubling the constraints of  $L$  and  $W$  given in Table 3, resulting in a four-fold size 15 of an average ellipsoid, decreases the computing time by 11 % whilst executing the model with halved values of  $L$  and  $W$ , leading to a quarter of the original average ellipsoid size, increases the computing time by 21 %.

## 5.2 Factor of safety and slope failure probability

Next, we compute FoS for shallow landslides in the study area with values of  $d_e = 100$ , 20 500, 2500, and 12 500. We evaluate the modelling results against observed shallow landslide areas (see Fig. 4). Larger values of  $d_e$  result in a more conservative prediction in terms of FoS – if more ellipsoids are tested, the chance is higher for each pixel that 25 at least one slip surface is associated with  $\text{FoS} < 1$  (Fig. 6). All tests result in a rather successful than unsuccessful prediction, even though the false prediction rates are significant. There is no optimum value for  $d_e$ , per se. Strictly speaking,  $d_e \sim \infty$  would be needed – as the rate of positive predictions may increase also at very high values 30 of  $d_e$ , there will always be a trade-off between the computing time and the quality of the results. However, we note that, in this example, the overall quality of the prediction does not increase with larger values of  $d_e$  (i.e., the polygon does not significantly shift 35 towards a successful prediction), indicating that most areas with  $\text{FoS} < 1$  were detected

at earlier stages of the computation, and the additional areas with  $\text{FoS} < 1$ , detected at later stages of the computation, consist equally in true positive and false positive predictions. For the purpose of the present study, we consider  $d_e = 2500$  a sufficiently reasonable approximation.

- We compute slope failure probability for a subset of the Collazzone area (see Fig. 4) with five different sample sizes, applying each of the sampling strategies (a), (b) and (c) introduced in Fig. 2.  $c'$ ,  $\varphi'$  and  $d$  are sampled. We assume that the accuracy of the results increases with increasing values of  $d_e$  and  $n$ . However, so does the computing time. Therefore, we attempt to identify those values where the results converge – i.e., the ideal values in terms of accuracy and time efficiency. We take the average value of  $P_f$  over the study area as reference. Figure 7a illustrates how the average value of  $P_f$  increases with increasing  $d_e$ . It further indicates the sample size  $n$  needed for convergence i.e., the value of  $n$  where the average  $P_f$  remains constant when  $n$  is further increased. Obviously, equal density sampling (c) performs best whilst random sampling of parameters (b) is not a valid alternative: with a very high number of tested ellipsoids, it is likely that at least one of the random samples is biased towards low values of  $c'$  and  $\varphi'$ . Therefore, on the logarithmic scale used in Fig. 7a, average  $P_f$  steadily increases with increasing  $d_e$ . This effect is less pronounced for larger values of  $n$ , but it could only be diminished by testing excessively large samples i.e., at the cost of a very long computing time. Sampling strategy (a), with randomly sampled parameter combinations, is less susceptible to these effects as the samples are better distributed within their range (see Fig. 2). Still, with the assumptions tested, the curves converge at a higher average of  $P_f$  and flatten out more slowly than the curves for equal density sampling. Further, strategy (a) is highly inefficient. With similar values of  $d_e$  and  $n$ , the computing time is roughly 20–25 times longer than for strategy (c). The reason for this phenomenon is that the number of truncated depths to be tested is  $n$  with strategy (a) and the cubic root of  $n$  with the other strategies. Hence, with (a), the geometry of a much larger number of slip surfaces has to be built than for (b) and (c), which is costly in terms of computing time.

<a href="#">Title Page</a>	
<a href="#">Abstract</a>	<a href="#">Introduction</a>
<a href="#">Conclusions</a>	<a href="#">References</a>
<a href="#">Tables</a>	<a href="#">Figures</a>
<a href="#">◀</a>	<a href="#">▶</a>
<a href="#">◀</a>	<a href="#">▶</a>
<a href="#">Back</a>	<a href="#">Close</a>
<a href="#">Full Screen / Esc</a>	
<a href="#">Printer-friendly Version</a>	
<a href="#">Interactive Discussion</a>	



Independently of the sampling strategy, the average slope failure probability decreases with the number of samples. For the strategies (a) and (b), this is a result of the lower tendency of outliers with larger sample sizes, which is more pronounced with (b) than with (a). With sampling strategy (c), it is a result of the fact that an exponential PDF is assumed for  $c'$ . With lower sample sizes, the relative weight of the minimum value  $c' = 0 \text{ kN m}^{-2}$  is higher than with higher values of  $n$ , resulting in higher values of  $P_f$ .

Among all the tests shown, we expect equal density sampling with  $n = 15^3$  to perform best in terms of accuracy. With  $d_e = 12\,500$ ,  $n = 15^3$  yields an average  $P_f = 0.094$ .  $n = 12^3$  and  $d_e = 12\,500$  yields an average  $P_f = 0.095$ . In a certain range, reducing  $n$  and  $d_e$  affects moderately the model results, but improves significantly the computational efficiency. Setting  $n = 9^3$  and  $d_e = 12\,500$  gives an average  $P_f = 0.097$ , saving 75 % of the computing time, and setting  $n = 9^3$  and  $d_e = 2500$  gives an average  $P_f = 0.090$ , saving 95 % of the computing time. Given the level of uncertainty in the geotechnical parameterization, reducing the values of  $n$  and  $d_e$  can be a strategy for the computation of very large areas, keeping the computing time within reasonable limits. Even though we do not recommend using values of  $n < 9^3$  and  $d_e < 2500$ , Fig. 7b shows that, within a certain range, changes of  $n$  and  $d_e$  do not affect significantly the capability of the model to reproduce the patterns of observed landslide/non-landslide areas in terms of the area under the ROC curve  $A_{\text{ROC}}$ . This indicates that changes of the results for larger values of  $n$  and  $d_e$  affect equally areas with low and high values of  $P_f$ .

Figure 8a illustrates the modelled distribution of FoS in the study area, and Fig. 8b portrays the spatial patterns of  $P_f$ .

## 6 Discussion

Exploiting multi-processor computing environments enables the execution of complex slope stability models for reasonably large areas within an acceptable amount of time.

Title Page

Abstract

Introduction

Conclusions

References

Tables

Figures

◀

▶

◀

▶

Back

Close

Full Screen / Esc

Printer-friendly Version

Interactive Discussion



This strategy allows testing large numbers of slip surfaces and looping over many combinations of geotechnical parameterizations. With equal density sampling of the parameters, a sample size of  $n \sim 15^3$  is sufficient to provide convergence of the probability of failure,  $P_f$ , results. These findings are valid for shallow landslides where three parameters ( $c'$ ,  $\varphi'$  and  $d$ ) are sampled.

With the reduction of computing time, the remaining key challenge for broad-scale slope stability modelling consists in the parameterization of the input data. The geotechnical parameterization used is considered reasonable for testing model performance. However, it calls for improvements with regard to more reliable landslide 10 susceptibility and hazard maps.

In the present work, we assume constant statistical properties ( $\mu$ ,  $\sigma$ , minimum, maximum) of the geotechnical parameters  $c'$  and  $\varphi'$  and of the soil depth  $d$  over the relevant part of the study area. Even though, in this specific case, we can well justify this generalization, it may be too simplistic in other cases.

We further assume independent statistical properties of  $c'$  and  $\varphi'$ . However, this is 15 a rough simplification as these parameters – representing the offset and inclination of the linear regression in the Mohr–Coulomb Diagram – are often negatively correlated. A future challenge will consist in finding an appropriate way to build PDFs considering the interdependency of the two parameters.

Finally, the PDFs that were used in the study may be improved. Whilst the density 20 functions for  $d$  and  $\varphi'$  are reasonably well supported by the empirical observations, the exponential PDF used for  $c'$  was derived for soils with a high content of sand and silt (El-Ramly et al., 2005; Petrovic, 2008). For clay, a log-normal function seems to better describe the observations. A joint, two-variable PDF depending on both  $c'$  and  $\varphi'$  may 25 be hypothesized. Such a function is expected to yield significantly less conservative results. Given a sufficiently large dataset, we suggest to use the PDF for  $\varphi'$  and couple the function for  $c'$  to the tested value of  $\varphi'$  (see Sect. 2). An appropriate geotechnical parameterization requires a detailed knowledge of the area under investigation. As an

example, if deep-seated slope stability is considered, this understanding should include the strike and dip directions of bedding planes (Santangelo et al., 2014).

## 7 Conclusions

We have described and tested r.slope.stability, a multi-core numerical GRASS GIS implementation of a 3-D slope stability model for large areas, highlighting (i) the gain in computing time, and the consequent applicability to large areas, and (ii) the possibility of modelling the spatial probability of slope failures, based on the natural variability of geotechnical characteristics of the soils. Using commonly available multi-core hardware, the use of parallel processing may reduce running times by a factor larger than 20. Our parallel implementation is transparent to the r.slope.stability user in GRASS GIS, since it is based on the automatic partitioning of the study area in tiles, processed in parallel. The modelling results are presented for the entire area, and validated against observed landslides.

We conclude that parallel processing enables the application of complex slope stability models for large areas in a reasonable amount of time. A remaining challenge for this type of task is the geotechnical parameterization of the area under investigation. In the present paper, we have demonstrated a simple approach to compute slope failure probabilities by using PDFs of  $c'$ ,  $\varphi'$ , and  $d$ . This approach is considered sufficient for the purpose of the present work. The model results reasonably correspond to the distribution of observed shallow landslides in the Collazzone area. However, we have identified a considerable potential for improvement with regard to (i) regionalization of the parameters, (ii) consideration of the interrelation of  $c'$  and  $\varphi'$  and (iii) optimization of the PDFs used.

**Acknowledgements.** The work was supported by grants of the Italian National Department for Civil Protection (DPC) and the Regione dell’Umbria (contract POR-FESR Umbria 2007–2013, asse ii, attività a1, azione 5). We further acknowledge the kind cooperation of F. Ardizzone, L.

[Title Page](#)[Abstract](#)[Introduction](#)[Conclusions](#)[References](#)[Tables](#)[Figures](#)[◀](#)[▶](#)[◀](#)[▶](#)[Back](#)[Close](#)[Full Screen / Esc](#)[Printer-friendly Version](#)[Interactive Discussion](#)

## References

- Alvioli, M., Rossi, M., and Guzzetti, F.: Scaling properties of rainfall-induced landslides predicted by a physically based model, *Geomorphology*, 213, 38–47, 2014.
- Ardizzone, F., Cardinali, M., Galli, M., Guzzetti, F., and Reichenbach, P.: Identification and mapping of recent rainfall-induced landslides using elevation data collected by airborne Lidar, *Nat. Hazards Earth Syst. Sci.*, 7, 637–650, doi:10.5194/nhess-7-637-2007, 2007.
- Ardizzone, F., Fiorucci, F., Santangelo, M., Cardinali, M., Mondini, A. C., Rossi, M., Reichenbach, P., and Guzzetti, F.: Very-high resolution stereoscopic satellite images for landslide mapping, in: *Landslide Science and Practice: Volume 1: Landslide Inventory and Susceptibility and Hazard Zoning*, edited by: Margottini, C., Canuti, P., and Sassa, K., Springer, Heidelberg, Berlin, New York, 95–101, 2013.
- Baum, R. L., Savage, W. Z., and Godt, J. W.: TRIGRS – a Fortran Program for Transient Rainfall Infiltration and Grid-Based Regional Slope-Stability Analysis, Version 2.0, USGS Open-File Rep. 2008-1159, 2008.
- Brabb, E. E.: Innovative approaches to landslide hazard and risk mapping, in: *Proceedings of the 4th International Symposium on Landslides*, Toronto, Ontario, Canada, 16–21 September 1984, 1, 307–324, 1984.
- Bishop, A. W.: The use of the slip circle in the stability analysis of slopes, *Geotechnique*, 5, 7–17, 1954.
- Burton, A. and Bathurst, J. C.: Physically based modelling of shallow landslide sediment yield at a catchment scale, *Environ. Geol.*, 35, 89–99, 1998.
- Cardinali, M., Ardizzone, F., Galli, M., Guzzetti, F., and Reichenbach, P.: Landslides triggered by rapid snow melting, the December 1996–January 1997 event in Central Italy, in: *Proceedings 1st Plinius Conference on Mediterranean Storms*, edited by: Claps, P. and Siccardi, F., Maratea, Italy, 14–16 October 1999, 439–448, 2000.
- Carson, M. A. and Kirkby, M. J.: *Hillslope Form and Process*, Cambridge University Press, London, 1972.

A strategy for  
GIS-based 3-D slope  
stability modelling

M. Mergili et al.

[Title Page](#)

[Abstract](#)

[Introduction](#)

[Conclusions](#)

[References](#)

[Tables](#)

[Figures](#)



[Back](#)

[Close](#)

[Full Screen / Esc](#)

[Printer-friendly Version](#)

[Interactive Discussion](#)



Coulomb, C. A.: Essais sur une application des règles des maximis et minimis à quelques problèmes de statique relatifs à l'architecture, Mémoirs présentées par divers Savants, Academie des Sciences Paris, 7, 343–387, 1776.

5 Crozier, M. J.: Landslides: Causes Consequences and Environment, Croom Helm, London, 1986.

Duncan, J. M. and Wright, S. G.: Soil Strength and Slope Stability, Wiley, Hoboken, NJ, 2005.

El-Ramly, H., Morgenstern, N. R., and Cruden, D. M.: Probabilistic assessment of stability of a cut slope in residual soil, *Geotechnique*, 55, 77–84, 2005.

10 Fellenius, W.: Erdstatische Berechnungen mit Reibung und Kohäsion (Adhäsion) und unter Annahme kreiszylindrischer Gleitflächen, W. Ernst & Sohn, Berlin, Germany, 1927.

Fiorucci, F., Cardinali, M., Carlà, R., Rossi, M., Mondini, A. C., Santurri, L., Ardizzone, F., and Guzzetti, F.: Seasonal landslides mapping and estimation of landslide mobilization rates using aerial and satellite images, *Geomorphology*, 129, 59–70, 2011.

15 Galli, M., Ardizzone, F., Cardinali, M., Guzzetti, F., and Reichenbach, P.: Comparing landslide inventory maps, *Geomorphology*, 94, 268–289, 2008.

Godt, J. W., Baum, R. L., Savage, W. Z., Salciarini, D., Schulz, W. H., and Harp, E. L.: Transient deterministic shallow landslide modeling: requirements for susceptibility and hazard assessments in a GIS framework, *Eng. Geol.*, 102, 214–226, 2008.

20 GRASS Development Team: GRASS GIS. The world's leading Free GIS software, Open Source Geospatial Foundation Project, available at: <http://grass.osgeo.org> (last access: 31 January 2014), 2014.

Griffiths, D. W., Huang, J., and de Wolfe, G. F.: Numerical and analytical observations on long and infinite slopes, *Int. J. Numer. Anal. Met.*, 35, 569–585, 2011.

25 Gruber, F. E. and Mergili, M.: Regional-scale analysis of high-mountain multi-hazard and risk indicators in the Pamir (Tajikistan) with GRASS GIS, *Nat. Hazards Earth Syst. Sci.*, 13, 2779–2796, doi:10.5194/nhess-13-2779-2013, 2013.

Guzzetti, F.: Landslide Hazard and Risk Assessment, Ph.D. thesis, University of Bonn, Germany, 2006.

30 Guzzetti, F., Carrara, A., Cardinali, M., and Reichenbach, P.: Landslide hazard evaluation: a review of current techniques and their application in a multi-scale study, Central Italy, *Geomorphology*, 31, 181–216, 1999.

Title Page

Abstract

Introduction

Conclusions

References

Tables

Figures



Back

Close

Full Screen / Esc

Printer-friendly Version

Interactive Discussion



- Guzzetti, F., Cardinali, M., Reichenbach, P., Cipolla, F., Sebastiani, C., Galli, M., and Salvati, P.: Landslides triggered by the 23 November 2000 rainfall event in the Imperia Province, Western Liguria, Italy, *Eng. Geol.*, 73, 229–245, 2004.
- Guzzetti, F., Galli, M., Reichenbach, P., Ardizzone, F., and Cardinali, M.: Landslide hazard assessment in the Collazzone area, Umbria, Central Italy, *Nat. Hazards Earth Syst. Sci.*, 6, 115–131, doi:10.5194/nhess-6-115-2006, 2006a.
- Guzzetti, F., Reichenbach, P., Ardizzone, F., Cardinali, M., and Galli, M.: Estimating the quality of landslide susceptibility models, *Geomorphology*, 81, 166–184, 2006b.
- Guzzetti, F., Ardizzone, F., Cardinali, M., Rossi, M., and Valigi, D.: Landslide volumes and landslide mobilization rates in Umbria, central Italy, *Earth Planet. Sc. Lett.*, 279, 222–229, 2009.
- Hovland, H. J.: Three-dimensional slope stability analysis method, *J. Geotech. Eng.-ASCE*, 103, 971–986, 1977.
- Hungr, O.: A extension of Bishop's simplified method of slope stability analysis to three dimensions, *Geotechnique*, 37, 113–117, 1987.
- Hungr, O.: CLARA: Slope Stability Analysis in Two or Three Dimensions, *Geotechnical Research*, Vancouver, British Columbia, Canada, 1988.
- Hungr, O., Salgado, F. M., and Byrne, P. M.: Evaluation of a three-dimensional method of slope stability analysis, *Can. Geotech. J.*, 26, 679–686, 1989.
- Iverson, R. M. and Major, J. J.: Groundwater seepage vectors and the potential for hillslope failure and debris flow mobilization, *Water Resour. Res.*, 22, 1543–1548, 1986.
- Janbu, N., Bjerrum, L., and Kjaernsli, B.: Soil Mechanics Applied to Some Engineering Problems, Publication 16, Norwegian Geotechnical Institute, Oslo, 1956.
- Jia, N., Mitani, Y., Xie, M., and Djamaruddin, I.: Shallow landslide hazard assessment using a three-dimensional deterministic model in a mountainous area, *Comput. Geotech.*, 45, 1–10, 2012.
- King, G.: Revision of effective-stress method of slices, *Geotechnique*, 39, 497–502, 1989.
- Kolymbas, D.: *Geotechnik: Bodenmechanik und Grundbau*, Springer, Berlin, Heidelberg, 2007.
- Lam, L. and Fredlund, D. G.: A general limit equilibrium model for 3-D slope stability analysis, *Can. Geotech. J.*, 30, 905–919, 1993.
- Marchesini, I., Cencetti, C., and de Rosa, P.: A preliminary method for the evaluation of the landslides volume at a regional scale, *Geoinformatica*, 13, 277–289, 2009.

## A strategy for GIS-based 3-D slope stability modelling

M. Mergili et al.

[Title Page](#)

[Abstract](#)

[Introduction](#)

[Conclusions](#)

[References](#)

[Tables](#)

[Figures](#)



[Back](#)

[Close](#)

[Full Screen / Esc](#)

[Printer-friendly Version](#)

[Interactive Discussion](#)



<a href="#">Title Page</a>	
<a href="#">Abstract</a>	<a href="#">Introduction</a>
<a href="#">Conclusions</a>	<a href="#">References</a>
<a href="#">Tables</a>	<a href="#">Figures</a>
<a href="#">◀</a>	<a href="#">▶</a>
<a href="#">◀</a>	<a href="#">▶</a>
<a href="#">Back</a>	<a href="#">Close</a>
<a href="#">Full Screen / Esc</a>	
<a href="#">Printer-friendly Version</a>	
<a href="#">Interactive Discussion</a>	

- Mergili, M., Fellin, W., Moreiras, S. M., and Stötter, J.: Simulation of debris flows in the Central Andes based on Open Source GIS: possibilities, limitations, and parameter sensitivity, *Nat. Hazards*, 61, 1051–1081, 2012a.
- Mergili, M., Schratz, K., Ostermann, A., and Fellin, W.: Physically-based modelling of granular flows with Open Source GIS, *Nat. Hazards Earth Syst. Sci.*, 12, 187–200, doi:10.5194/nhess-12-187-2012, 2012b.
- Mergili, M., Marchesini, I., Rossi, M., Guzzetti, F., and Fellin, W.: Spatially distributed three-dimensional slope stability modelling in a raster GIS, *Geomorphology*, 206, 178–195, 2014.
- Milledge, D., Griffiths, V., Lane, S., and Warburton, J.: Limits on the validity of infinite length assumptions for modelling shallow landslides, *Earth Surf. Proc. Land.*, 37, 1158–1166, 2012.
- Montgomery, D. R. and Dietrich, W. E.: A physically based model for the topographic control on shallow landsliding, *Water Resour. Res.*, 30, 1153–1171, 1994.
- Morgenstern, N. R. and Price, V. E.: A numerical method for solving the equations of stability of general slip surfaces, *Comput. J.*, 9, 388–393, 1967.
- Munro, A. S. and Liao, H.-J.: Rainfall infiltration: infinite slope model for landslides triggering by rainstorm, *Nat. Hazards*, 54, 967–984, 2010.
- Neteler, M. and Mitasova, H.: Open Source GIS: a GRASS GIS Approach, Springer, New York, 2007.
- Pack, R. T., Tarboton, D. G., and Goodwin, C. N.: The SINMAP approach to terrain stability mapping, 8th Congress of the International Association of Engineering Geology, Vancouver, British Columbia, 1998.
- Petrovic, I.: Probabilistic stability analysis of sanitary landfill Jakusevec, in: Proceedings of the 1st Middle European Conference on Landfill Technology, Budapest, Hungary, 6–8 February 2008, 2008.
- Pyke, R.: TSLOPE3: Users Guide, Taga Engineering System and Software, Lafayette, LA, 1991.
- Prinz, H. and Strauss, R.: Ingenieurgeologie, 5th edn., Spektrum Akademischer Verlag, Heidelberg, Germany, 2011.
- Raia, S., Alvioli, M., Rossi, M., Baum, R. L., Godt, J. W., and Guzzetti, F.: Improving predictive power of physically based rainfall-induced shallow landslide models: a probabilistic approach, *Geosci. Model Dev.*, 7, 495–514, doi:10.5194/gmd-7-495-2014, 2014.



## A strategy for GIS-based 3-D slope stability modelling

M. Mergili et al.

[Title Page](#)

[Abstract](#)

[Introduction](#)

[Conclusions](#)

[References](#)

[Tables](#)

[Figures](#)

[◀](#)

[▶](#)

[◀](#)

[▶](#)

[Back](#)

[Close](#)

[Full Screen / Esc](#)

[Printer-friendly Version](#)

[Interactive Discussion](#)



R Core Team.: R: a Language and Environment for Statistical Computing, R Foundation for Statistical Computing, Vienna, Austria, available at: <http://www.R-project.org> (last access: 31 January 2014), 2014.

Reid, M. E., Christian, S. B., and Brien, D. L.: Gravitational stability of three-dimensional strato-volcano edifices, *J. Geophys. Res.*, 105, 6043–6056, 2000.

Rossi, M., Guzzetti, F., Reichenbach, P., Mondini, A. C., and Peruccacci, S.: Optimal landslide susceptibility zonation based on multiple forecasts, *Geomorphology*, 114, 129–142, 2010.

Santangelo, M., Marchesini, I., Cardinali, M., Fiorucci, F., Rossi, M., Bucci, F., and Guzzetti, F.: A method for the assessment of the influence of bedding on landslide abundance and types, *Landslides*, doi:10.1007/s10346-014-0485-x, 2014.

Van Westen, C. J.: The modelling of landslide hazards using GIS, *Surv. Geophys.*, 21, 241–255, 2000.

Van Westen, C. J. and Terlien, M. T. J.: An approach towards deterministic landslide hazard analysis in GIS. A case study from Manizales (Colombia), *Earth Surf. Proc. Land.*, 21, 853–868, 1996.

Van Westen, C. J., Van Asch, T. W. J., and Soeters, R.: Landslide hazard and risk zonation – why is it still so difficult?, *B. Eng. Geol. Environ.*, 65, 167–184, 2006.

Wilkinson, P. L., Anderson, M. G., and Lloyd, D. M.: An integrated hydrological model for rainfall-induced landslide prediction, *Earth Surf. Proc. Land.*, 27, 1285–1297, 2002.

Xie, M., Esaki, T., Zhou, G., and Mitani, Y.: Three-dimensional stability evaluation of landslides and a sliding process simulation using a new geographic information systems component, *Environ. Geol.*, 43, 503–512, 2003.

Xie, M., Esaki, T., and Cai, M.: A time-space based approach for mapping rainfall-induced shallow landslide hazard, *Environ. Geol.*, 46, 840–850, 2004a.

Xie, M., Esaki, T., and Cai, M.: A GIS-based method for locating the critical 3D slip surface in a slope, *Comput. Geotech.*, 31, 267–277, 2004b.

Xie, M., Esaki, T., and Zhou, G.: GIS-based probabilistic mapping of landslide hazard using a three-dimensional deterministic model, *Nat. Hazards*, 33, 265–282, 2004c.

Xie, M., Esaki, T., Qiu, C., and Wang, C.: Geographical information system-based computational implementation and application of spatial three-dimensional slope stability analysis, *Comput. Geotech.*, 33, 260–274, 2006.

---

A strategy for  
GIS-based 3-D slope  
stability modelling

M. Mergili et al.

---

[Title Page](#)

[Abstract](#)

[Introduction](#)

[Conclusions](#)

[References](#)

[Tables](#)

[Figures](#)



[Back](#)

[Close](#)

[Full Screen / Esc](#)

[Printer-friendly Version](#)

[Interactive Discussion](#)



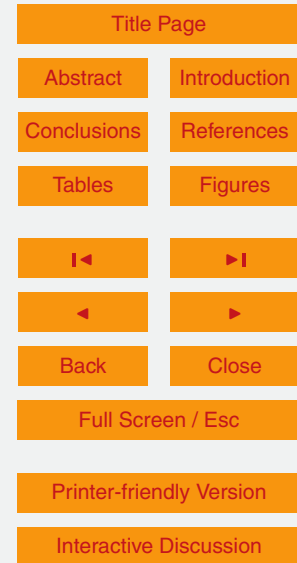
---

**A strategy for  
GIS-based 3-D slope  
stability modelling**

M. Mergili et al.

**Table 1.** 5th and 95th percentiles of length  $L$ , width  $W$ , and the  $L/W$  ratio for selected shallow landslides mapped in the Collazzone area.  $L$  is measured in the direction of the steepest slope.

Percentile	$L$ (m)	$W$ (m)	$L/W$
5th	16	15	0.38
95th	129	125	2.85



## A strategy for GIS-based 3-D slope stability modelling

M. Mergili et al.

**Table 2.** Geotechnical key parameters derived for 13 samples from the Collazzone study area (see Fig. 4 for location of the sites).  $\gamma_d$  = dry specific weight ( $\text{kN m}^{-3}$ ),  $c'$  = effective cohesion ( $\text{kN m}^{-2}$ ),  $\varphi'$  = effective angle of internal friction (degree). Arithmetic mean  $\mu$  and standard deviation  $\sigma$  are listed. \* For the exponential distribution applied to cohesion, the standard deviation is equal to the mean.

ID	$\gamma_d$	$c'$	$\varphi'$	USDA class
1	17.5	0.0	40.1	no data
2	15.3	0.0	33.6	no data
3	14.7	0.0	31.8	sand
4	15.8	24.5	25.9	sandy loam
5	16.8	2.8	30.1	loam
6	no data	4.5	35.1	loamy sand
7	17.6	0.0	35.4	no data
8	16.2	11.0	21.3	silty clay
9	15.8	5.7	26.5	silty clay
10	15.9	13.1	42.4	silty clay
11	15.6	6.7	27.6	clay loam
12	14.3	8.3	18.1	no data
13	14.6	13.2	20.5	silty clay
$\mu$	15.8	6.9	29.9	
$\sigma$	1.0	7.2*	7.5	

Title Page

Abstract

Introduction

Conclusions

References

Tables

Figures

◀

▶

◀

▶

Back

Close

Full Screen / Esc

Printer-friendly Version

Interactive Discussion



**Table 3.** Constraints and assumed statistical distribution of geotechnical parameters and soil depth for the generation of a slope failure probability  $P_f$  map.  $c'$  = effective cohesion ( $\text{kN m}^{-2}$ ),  $\varphi'$  = effective angle of internal friction (degree),  $d$  = soil depth (m).

	$c'$	$\varphi'$	$d$
Minimum	0.0	18.1	0.10
Maximum	24.5	42.4	1.22
Assumed distribution	Exponential	Log-normal	Log-normal



## A strategy for GIS-based 3-D slope stability modelling

M. Mergili et al.

[Title Page](#)

[Abstract](#)

[Introduction](#)

[Conclusions](#)

[References](#)

[Tables](#)

[Figures](#)



[Back](#)

[Close](#)

[Full Screen / Esc](#)

[Printer-friendly Version](#)

[Interactive Discussion](#)



**Table 4.** Parameters tested for their influence on model performance. Subscripts  $x$  and  $y$  refer to the  $x$  and  $y$  directions.

Parameter	Description	Tested values
Pixel size $d_x = d_y$ (m)	Length of one side of one pixel, all pixels have square shapes	5, 10, 20, 40
“Density of ellipsoids” $d_e$	Average number of tested ellipsoids touching each pixel	100, 500, 2500, 12 500
Ellipsoid size	Constraints for the randomization of ellipsoid dimensions	See text for details
Sample size $n$ (number of tested values of $c'$ , $\varphi'$ and $d'$ )	Number of samples used for computing $P_f$	$3^3$ (27), $6^3$ (216), $9^3$ (729), $12^3$ (1728), $15^3$ (3375)
Sampling strategy	Strategy for parameter sampling for $P_f$	Fig. 2a–c
Number of tiles $t$	Number of tiles the study area is divided into ( $t_x \times t_y$ )	1, 2 ( $1 \times 2$ ), 6 ( $2 \times 3$ ), 12 ( $3 \times 4$ ), 20 ( $4 \times 5$ ), 30 ( $5 \times 6$ ), 42 ( $6 \times 7$ ), 56 ( $7 \times 8$ ), 72 ( $8 \times 9$ ), 90 ( $9 \times 10$ ), 110 ( $10 \times 11$ ), 132 ( $11 \times 12$ ), 156 ( $12 \times 13$ ), 182, ( $13 \times 14$ ), 210 ( $14 \times 15$ ), 240 ( $15 \times 16$ )
Number of processors $p$	Number of processors to be used for the computation	1, 2–42 in steps of 2

# A strategy for GIS-based 3-D slope stability modelling

M. Mergili et al.

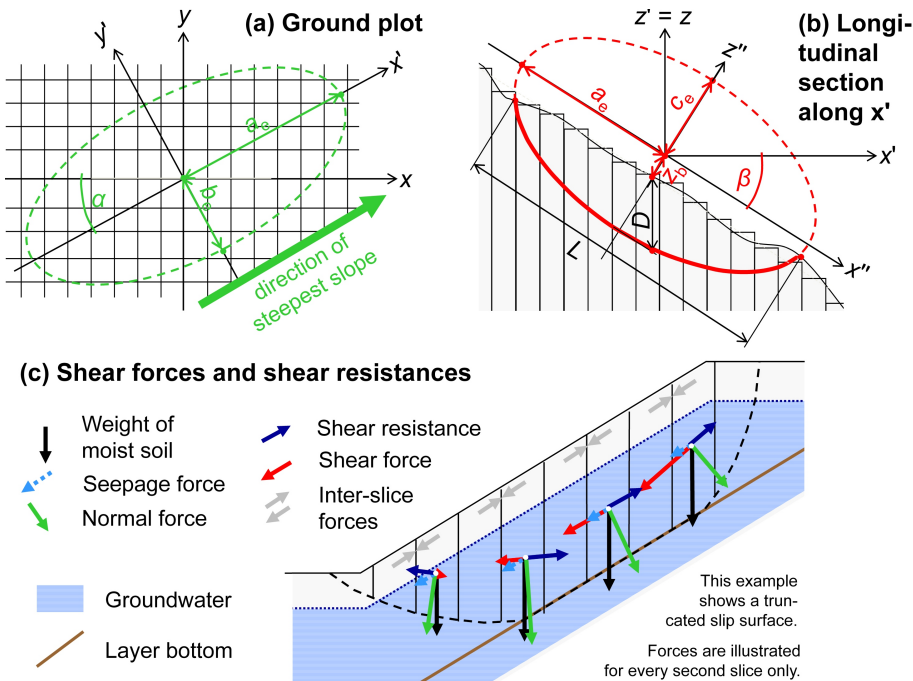


**Figure 1.** Typical ellipsoid used as slip surface in r.slope.stability. **(a)** Ground plot. **(b)** Longitudinal section. **(c)** Forces acting at each column. The factor of safety is computed for the ellipsoid bottom and (as shown in the figure) for the combination of the ellipsoid bottom and each intersecting layer bottom. The geotechnical, hydraulic and geometric details are outlined by Mergili et al. (2014).

Title Page

## Abstract

## Introduction

## Conclusions

## References

Tables

Figures



Back

Close

Full Screen / Esc

[Printer-friendly Version](#)

## Interactive Discussion

# A strategy for GIS-based 3-D slope stability modelling

M. Mergili et al.

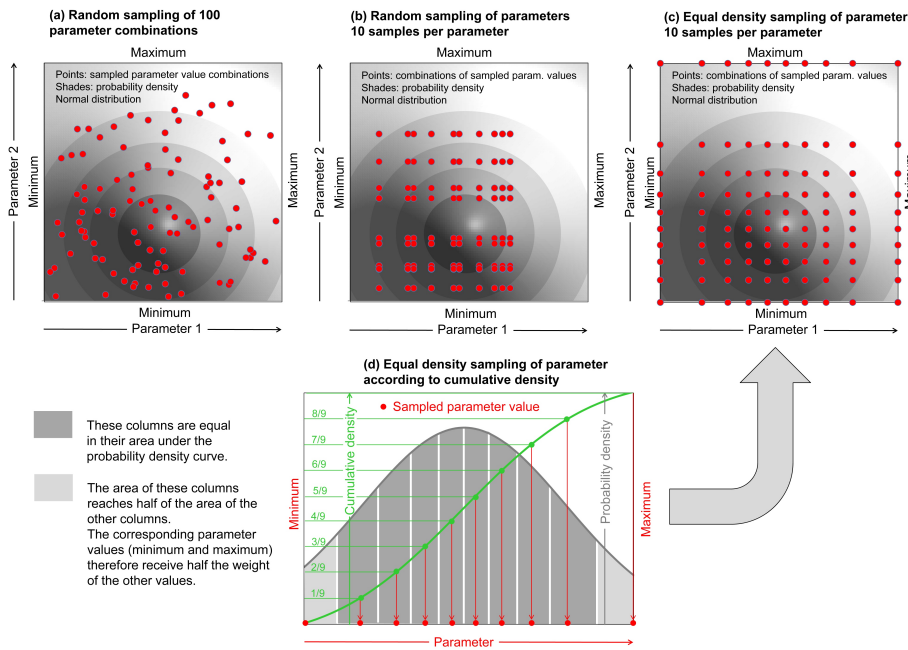


**Figure 2.** Sampling of parameters for computing slope failure probability. We test the sampling strategies **(a)**, **(b)**, and **(c)**. For clarity, sampling of two normally distributed arbitrary parameters is shown. In reality, we sample three parameters ( $c'$ ,  $\varphi'$  and truncated depth) according to different types of statistical distributions (see Sect. 4 for details). **(d)** illustrates how the cumulative density function is employed for equal density sampling.

Title Page

## Abstract

## Introduction

## Conclusions

## References

Table

Figures



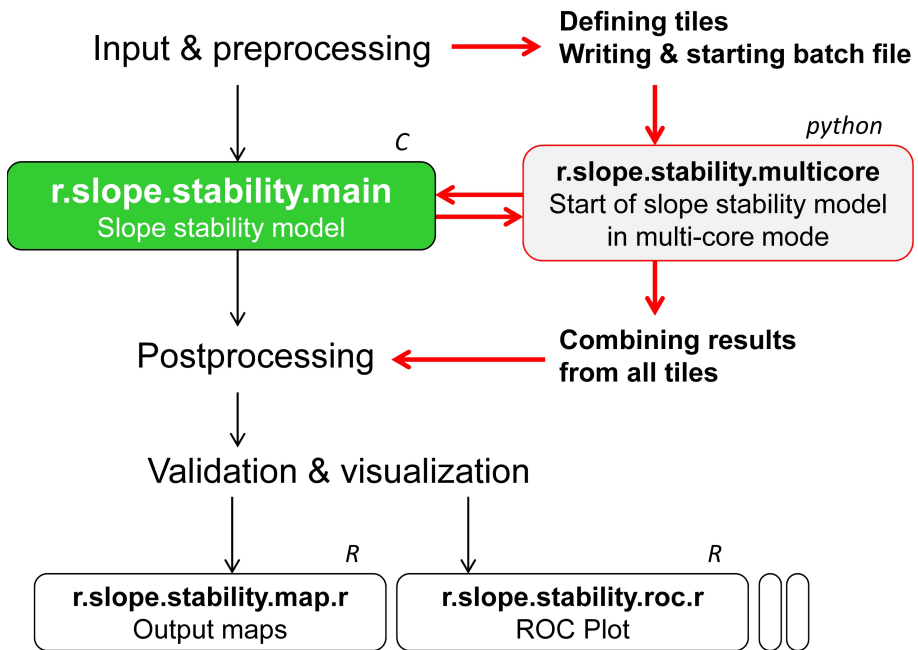


**Figure 3.** Logical framework of r.slope.stability. Plain text denotes steps directly implemented in the module r.slope.stability, and text in boxes denotes sub-modules. Italic letters indicate the programming environment used for the modules.

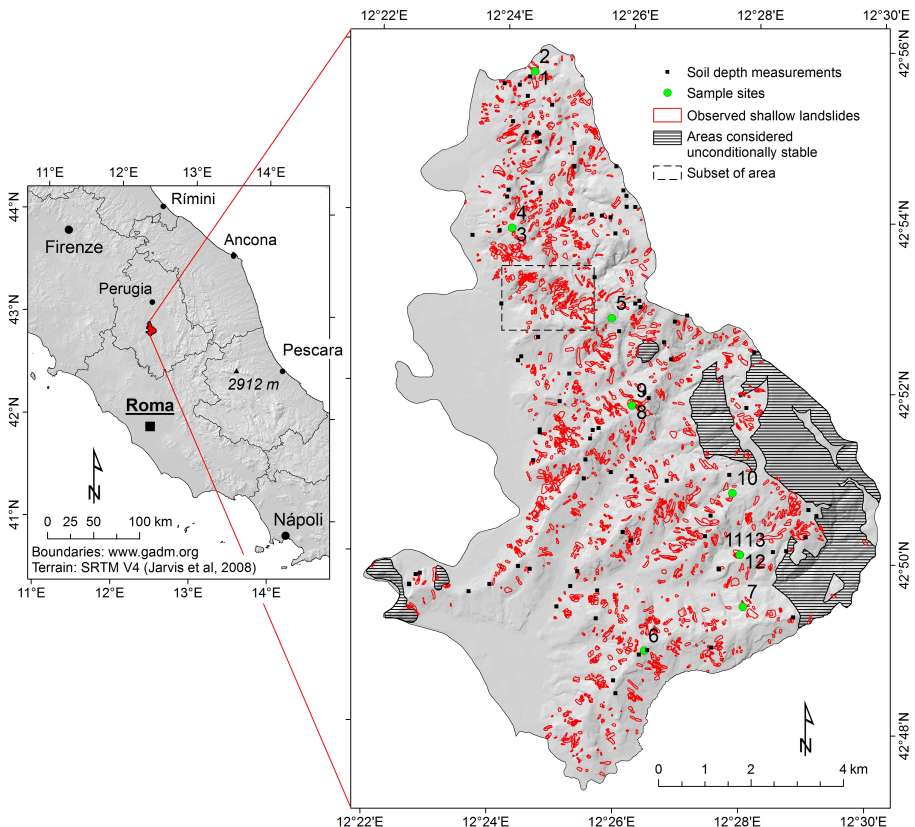


**Figure 4.** Collazzone study area, Umbria, central Italy. IDs of sample points correspond to IDs listed in Table 2.

Title Page

## Abstract

## Introduction

## Conclusions

## References

## Tables

## Figures



# A strategy for GIS-based 3-D slope stability modelling

M. Mergili et al.

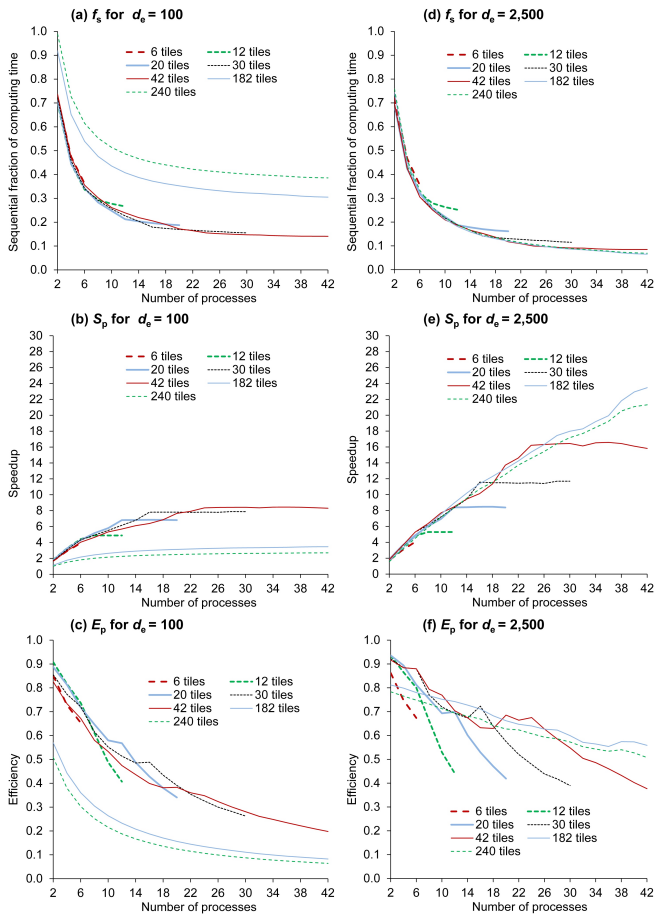


**Figure 5.** The serial fraction of code,  $f_s$ , speedup,  $S_p$ , and efficiency,  $E_p$ , plotted against the number of processes  $p$  for different values of the number of tiles  $t$  and average number of ellipsoids per pixel,  $d_e$ . See text for further explanations.

**Figure 6.** Influence of  $d_e$  on the performance of r.slope.stability in terms of prediction rates, building on FoS. Pixels representing observed shallow landslide areas (observed positives, OP) with a modelled value of  $\text{FoS} < 1$  represent true positive predictions (TP). OP pixels with  $\text{FoS} \geq 1$  represent false negative predictions (FN). Pixels not representing observed shallow landslide areas (observed negatives, ON) with a modelled value of  $\text{FoS} < 1$  represent false positive predictions (FP). Finally, ON pixels with  $\text{FoS} \geq 1$  represent true negative predictions (TN).

## A strategy for GIS-based 3-D slope stability modelling

M. Mergili et al.

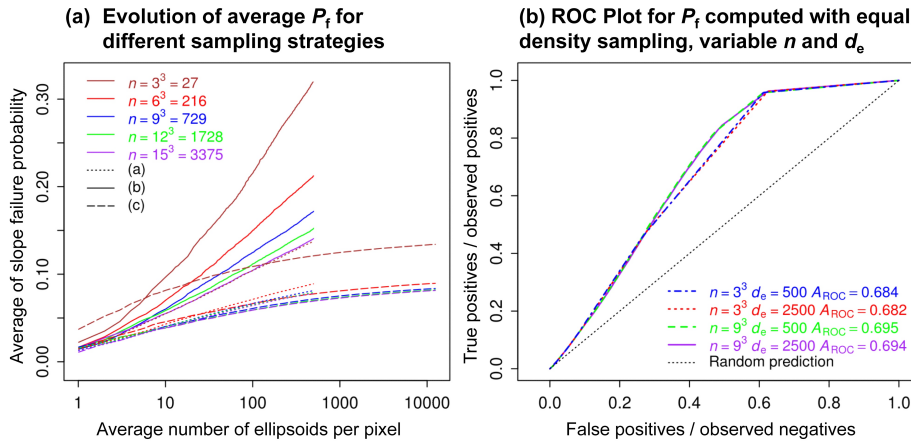


**Figure 7.** Slope failure probability computed with `r.slope.stability`. **(a)** Evolution of  $P_f$  for a subset of the Collazzone study area (see Fig. 4) with increasing value of  $d_e$ . The outcomes of the sampling strategies **(a)**, **(b)** and **(c)** introduced in Fig. 2 are compared. **(b)** ROC plot relating  $P_f$  to the observed shallow landslide areas in the entire Collazzone study area for different values of  $n$  and  $d_e$ .

- [Title Page](#)
- [Abstract](#) [Introduction](#)
- [Conclusions](#) [References](#)
- [Tables](#) [Figures](#)
- [◀](#) [▶](#)
- [◀](#) [▶](#)
- [Back](#) [Close](#)
- [Full Screen / Esc](#)
- [Printer-friendly Version](#)
- [Interactive Discussion](#)



# A strategy for GIS-based 3-D slope stability modelling

M. Mergili et al.

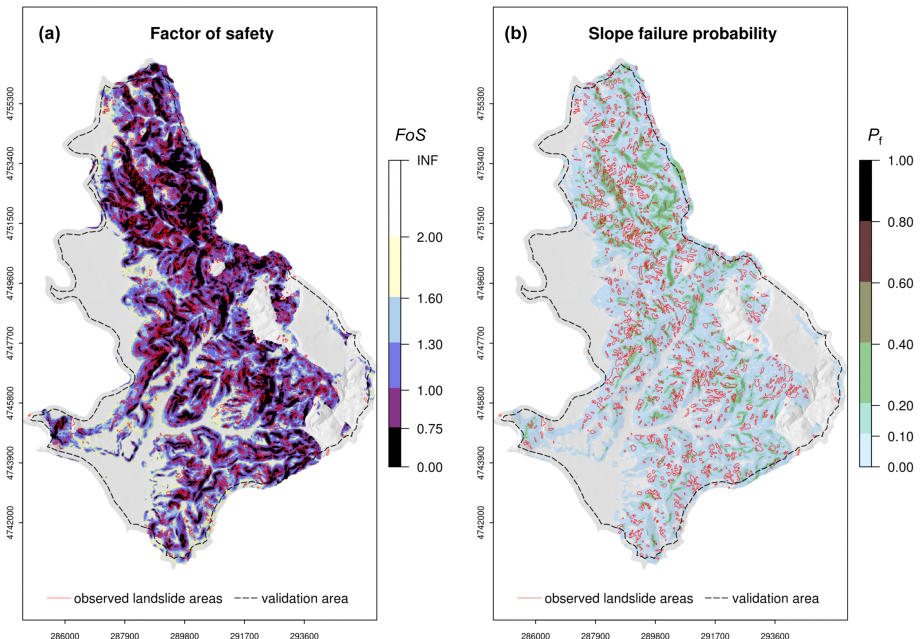


**Figure 8.** Spatial patterns of shallow slope stability in the Collazzone study area, computed with r.slope.stability. **(a)** FoS for  $d_e = 2500$ . **(b)**  $P_f$  for  $d_e = 2500$  and  $n = 9^3$ .

Title Page

## Abstract

## Introduction

## Conclusions

## References

Tables

## Figures



Back

Close

Full Screen / Esc

[Printer-friendly Version](#)

## Interactive Discussion

